Identifying the character of ferromagnetic Mn in epitaxial Fe/(Ga,Mn)As heterostructures

M. Sperl,[1] F. Maccherozzi,[2] F. Borgatti,[3] A. Verna,[4] G. Rossi,[4,5] M. Soda,[1] D. Schuh,[1] G. Bayreuther,[1] W. Wegscheider,[1] J. C. Cezar,[6] F. Yakhou,[6] N. B. Brookes,[6] C. H. Back,[1] and G. Panaccione[4,*]

[1]*Institut für Experimentelle Physik, Universität Regensburg, D-93040 Regensburg, Germany*

[2]*Soleil Synchrotron, L'Orme des Merisiers Saint-Aubin, BP 48, F-91192 Gif-sur-Yvette, France*

[3]*ISMN-CNR, via Gobetti 101, Bologna, Italy*

[4]*Laboratorio Nazionale TASC, INFM-CNR, in Area Science Park, S.S. 14, Km 163.5, I-34012 Trieste, Italy*

[5]*Dipartimento di Fisica, Università di Modena e Reggio Emilia, Via A. Campi 231/A, I-41100 Modena, Italy*

[6]*European Synchrotron Radiation Facility, BP 220, F-38043 Grenoble, France*

(Received 18 November 2009; revised manuscript received 22 December 2009; published 27 January 2010)

We demonstrate that the growth of Fe/(Ga,Mn)As heterointerfaces can be efficiently controlled by epitaxy and that robust ferromagnetism of the interfacial Mn atoms is induced at room temperature by the proximity effect. X-ray magnetic circular dichroism and x-ray resonant reflectivity data, supported by theoretical calculations, were used to monitor both temperature and magnetic field dependence of the Mn magnetic moment in the semiconducting host. We identify distinct Mn populations, each of them with specific magnetic character.

DOI: 10.1103/PhysRevB.81.035211 PACS number(s): 75.50.Pp, 71.20.Nr, 78.70.Dm

I. INTRODUCTION

Diluted magnetic semiconductors (DMS) hold promises for integrating spin control in electronic devices.[1,2] Although the correlation between magnetic and transport properties in DMS is known to be a crucial ingredient toward possible applications, the physical mechanisms governing both the magnetic character and the magnetization alignment of the metallic dopants in the semiconducting environment are open challenges of present DMS research.[3–5] One further key subject arises from the Curie temperature, presently around 200 K in the most representative DMS material (Ga,Mn)As (Ref. 6) while ferromagnetic (FM) behavior well beyond room temperature (RT) would be required in future spintronics devices. A promising direction that goes beyond conventional methodologies is to tailor novel properties by exploiting interface effects in highly controlled heterostructures (HS), as extensively demonstrated in oxide-based materials.[7–9] Following this approach, recent experimental efforts aimed at tuning specific magnetic properties in FM metal/DMS-based interfaces. In the case of direct exchange-coupled HS, the investigation of spin valve effect in MnAs/(Ga,Mn)As at low temperature (4.2 K) found the apparent formation of a inhomogeneous magnetic spring in the (Ga,Mn)As region[10] and a decrease in exchange coupling after insertion of a spacer layer [MnAs/*p*-GaAs/(Ga,Mn)As].[11] Differently, HS with 3*d* FM metals revealed (i) independent magnetization switching in $(Ni_{80}Fe_{20})/(Ga,Mn)As$, despite direct contact[12] and (ii) FM behavior of Mn at RT at nonepitaxial Fe/(Ga,Mn)As interfaces, with antiparallel alignment of the Fe and Mn moments.[13] A firm understanding of the mechanisms involved in these effects requires on one side a full control of HS growth and on the other side the ability to probe the electronic and magnetic properties in a chemical and depth sensitive way. Here we report polarization-dependent x-ray experiments on fully epitaxial Fe/(Ga,Mn)As HS, where we are able to follow the field, temperature, and depth evolution of the different magnetic configurations of the Mn ions. Our results reveal the presence of a electronic configuration of the Mn ions under the proximity effect of the Fe overlayers, indicating that (a) Mn hybridization is playing a fundamental role in the magnetic properties of the system and (b) paramagnetic and ferromagnetic Mn (antiparallel to Fe) have distinct spectroscopic fingerprints in an applied magnetic field, i.e., the different magnetic behavior in a sizeable part of the Mn atoms at the interface ($\gtrsim 1$ nm) is "switched on" by the Fe overlayer.

II. EXPERIMENTAL DETAILS

The ferromagnetic (Ga,Mn)As samples (Mn 3–8 % doping, 50–150 nm thick) have been grown by molecular-beam epitaxy (MBE). The rate for the low-temperature growth was about 0.6 Å/s (230°–250 °C). Subsequently the samples were transferred to a metal MBE for Fe evaporation. An optimized protocol to obtain contamination free and ordered surfaces was used, by combining low-temperature ultrahigh vacuum annealing (150 °C) and soft Ar^+ sputtering (500 eV, 45° incidence angle) for a typical time of 30 min. Details are given elsewhere.[14,15] Reference samples were obtained by HCl etching. The Fe growth rate was controlled *in situ* by quartz monitors and the Fe overlayers were prepared as stepped wedges with discrete thickness values to ensure that the growth conditions were identical for all thicknesses in the covered range from 0 to 23 ML. The resulting well ordered surfaces were verified by reflective high-energy electron diffraction. Samples were covered by a 8-nm-thick epitaxial Au(001) layer to prevent oxidation. The magnetic anisotropy axis of both Fe and (Ga,Mn)As layer, determined by a superconducting quantum interference device magnetometer and by magneto-optical Kerr effect (MOKE), closely resembles Fe/GaAs(001) and the nontreated (Ga,Mn)As/GaAs(001), respectively, excluding sizeable variations in the magnetic properties after the Ar^+ bombardment.[14–16] Moreover, the Curie temperature of the sputtered (Ga,Mn)As is identical to the one of the as-grown samples ($T_c = 67 \pm 3$ K). Figure 1(a) presents MOKE results. At the wavelength used the Kerr

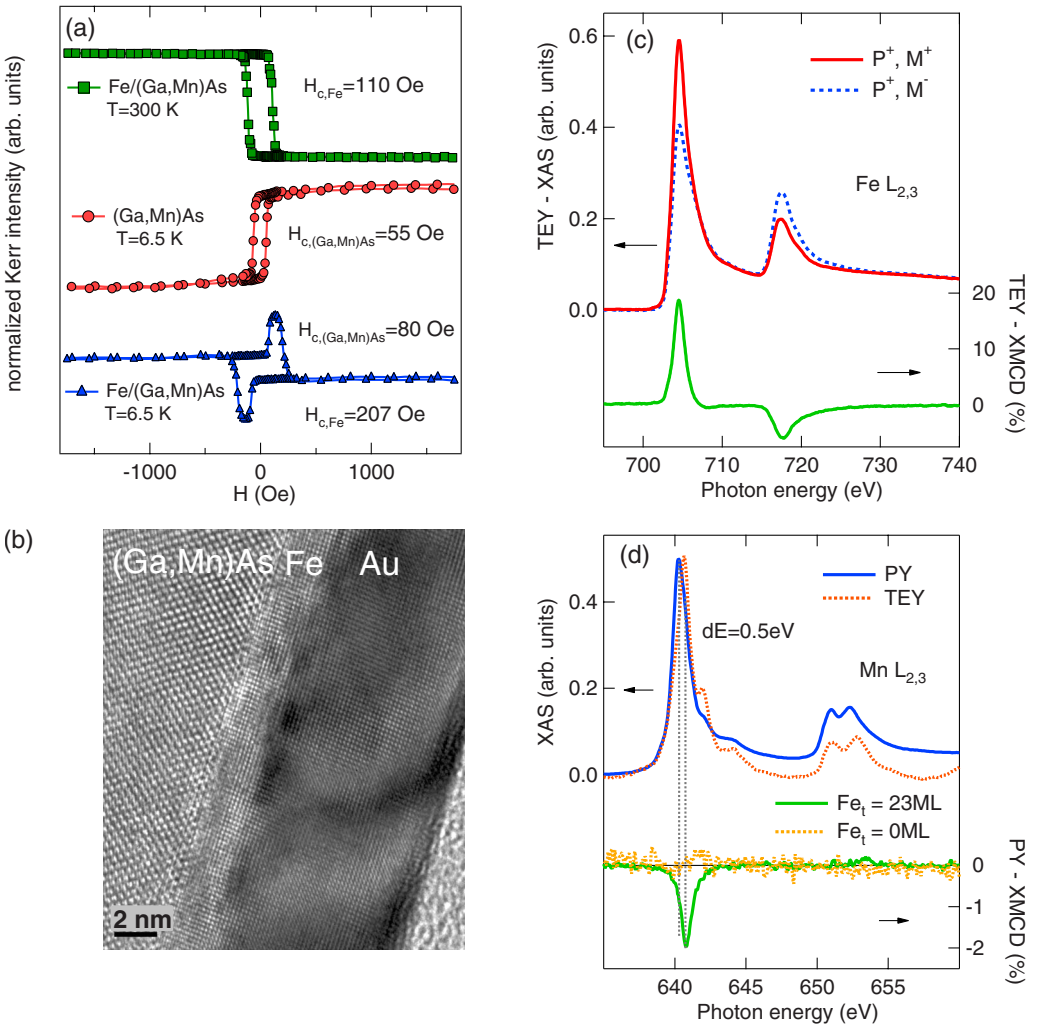

FIG. 1. (Color online) (a) Normalized MOKE data measured at 300 and 6.5 K for Fe/(Ga,Mn)As and (Ga,Mn)As. The Kerr contrast (measured with $\lambda=632$ nm) is opposite for Fe and (Ga,Mn)As which makes it possible to easily distinguish the two layers. The coercive field of Fe increases when going to lower temperatures as expected. A slight increase in H_c is observed for the pure (Ga,Mn)As when Fe is deposited on top. (Panel b) High-resolution cross-sectional TEM image of the epitaxial Fe(2 nm)/(Ga,Mn)As(50 nm) sample, capped with 8 nm of Au. The interface region is sharp and no intermixing is visible. The black horizontal line (bottom right) indicates the scale (2 nm). (Panel c) Fe $L_{2,3}$ edge spectra as measured in TEY mode ($T=120$ K, $H=0.04$ T, Fe=23 ML), with circular polarization (P^+) and opposite magnetization (M^+, M^-). Black arrows indicate the XAS (left) and XMCD (right) scale, respectively. (Panel d) Mn $L_{2,3}$ edge spectra as measured in TEY and PY mode ($T=120$ K, $H=0.04$ T, Fe=23 ML). Black arrows indicate the XAS (left) and XMCD (right) scale. Mn XAS spectra acquired in PY mode (blue/dark gray continuous line) and TEY mode (red/gray points) differ by 0.5 eV and display different fine structure at L_3 edge. XMCD signal at the Mn L_3 edge (green/light gray curve) is observed, indicating antiparallel magnetic coupling of Mn with respect to the Fe. No XMCD signal is measured in absence of the Fe overlayer (yellow/light gray curve in panel d, Fe=0 ML).

contrast for (Ga,Mn)As and Fe has opposite sign which makes it easy to separate the switching behavior of the two different layers. We show data at 300 K where only the Fe film produces a magnetic contrast and at 6.5 K for the Fe/GaMnAs film and for a pure (Ga,Mn)As film for comparison. We acquired x-ray absorption spectroscopy (XAS) and x-ray circular magnetic dichroism (XMCD) spectra at the Mn and Fe L edges at the ID08 dragon beamline (ESRF, France) and at the APE beamline of the Elettra Synchrotron (Trieste, Italy) in a temperature range of 10–300 K and a base vacuum $<5\times10^{-10}$ mbar. Total electron yield (TEY) and photon yield (PY, bulk sensitivity >40 nm) were acquired simultaneously. All spectra were normalized by the intensity of the incident beam. The TEY Fe XAS signal has been corrected for saturation effects, whereas PY mode has been preferred for Mn, due to both the need of bulk sensitivity and to the dilution in GaAs, resulting in negligible self-absorption effects of the fluorescence signal. X-ray resonant magnetic scattering (XRMS) measurements have been carried out at ID08 in specular reflection geometry by fixing the incoming photon energy at the L_3 Mn absorption peak and scanning the grazing angle θ from 0° to 40°. Right circularly polarized radiation was used and reflectivity measurements were performed in remanence after having applied the magnetic field in opposite directions. Simulation and fitting of the x-ray resonant reflectivity measurements have

been performed using the Pythonic Programming for Multilayer (PPM) software.[17,18]

III. RESULTS AND DISCUSSION

Figure 1 depicts the magnetic and structural characteristics of the Fe/(Ga,Mn)As HS. The crystallinity of the Au/Fe/(GaMn)As stack is confirmed by the transmission electron microscopy (TEM) image (panel b), revealing a sharp interface between Fe and (Ga,Mn)As. Reference XAS-XMCD signals from the Fe $L_{2,3}$ and Mn $L_{2,3}$ edges are displayed in panels (c) and (d), for 23 ML Fe and 0.04 T at 120 K, i.e., well above T_c of the (Ga,Mn)As substrate. The PY spectrum is located at ≅0.5 eV lower binding energy (BE) and it is less structured than the TEY one. The PY-XMCD displays FM behavior and antiparallel (AP) Mn orientation.[13] We stress that, above T_c, a XMCD signal at Mn $L_{2,3}$ edge is measured only in presence of the Fe overlayer. The yellow curve in panel (d) shows no XMCD at the Mn edge in the region free of Fe, thus indicating a magnetic behavior switched on by the proximity effect of the Fe film.

From spectroscopic results, it is generally agreed that the two prevailing Mn electronic structures in (Ga,Mn)As are Mn_{Ga} (Mn substitutional on the Ga site) and Mn forming oxides or aggregates near the surface, with a hybrid d^4-d^5-d^6 and a purely d^5 electronic configuration (localized Mn), respectively. The latter configuration has a more structured XAS spectrum, located at higher BE with respect to the d^4-d^5-d^6 one.[19–22] A recent detailed study on the depth concentration of Mn in (Ga,Mn)As reveals the presence of Mn with d^5 configuration up to 6 nm from the interface, coexisting with Mn_{Ga} and not related to oxide.[23] Results in Fig. 1, obtained on controlled epitaxial systems with negligible oxide contribution indicate a surface-interface region with d^5-like character (TEY spectrum) and a bulk region, mainly representative of the Mn_{Ga} (PY spectrum). For the sake of simplicity, we will refer in the following to Mn-1 (Mn_{Ga} substitutional), Mn-2 (d^5-like Mn), and to Mn-AP (FM Mn antiparallel to Fe). The evolution of the Mn $L_{2,3}$ XMCD signal vs applied magnetic field is presented in Fig. 2(a) (T=120 K, Fe 23 ML). At low field (0.04 T) only the Mn-AP dichroic component is visible at the L_3 edge, confirming previous results.[13] Increasing the field, further components appear at lower BE, evolving in a structured line shape with a double peak at the L_2 edge and with the magnetization aligned parallel to the field. These components correspond to the paramagnetic contribution of Mn-1. The XAS/XMCD arising from Mn-1 has been associated to a mixed-valence ground state due to the large Mn 3d hybridization with the surrounding 4sp states.[19,24,25] Numerical calculations indicated a mixed 80% d^5-20% $d^6\underline{L}$ ground state ($\underline{L}$ is a ligand hole).[24,25] In Mn-AP, both the energy shift of the XMCD minimum and the line shape suggest a different valence state with lower occupancy of the 3d levels, implying a lowering of the d^6 character and increment of the d^5 one.

In Fig. 2(b) the Mn-AP XMCD at 0.04 T is compared to atomic multiplet calculations, namely, a pure Mn d^5 ground-state configuration based on the ligand field model, for an

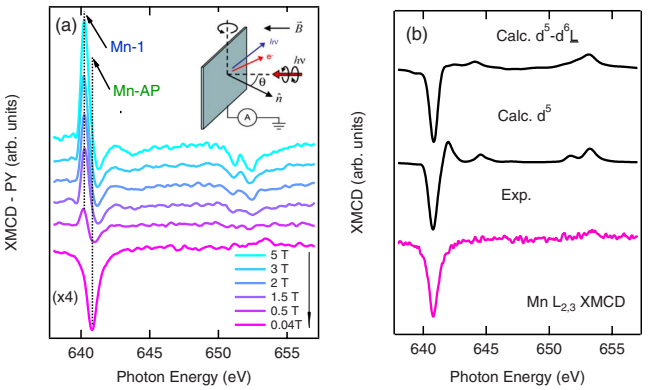

FIG. 2. (Color online) (Panel a) Evolution of the Mn XMCD line shape vs applied magnetic field (T=120 K, Fe=23 ML), measured in PY mode. The inset shows a sketch of the experimental geometry. (Panel b) Comparison of calculated and experimental (120 K, 0.04 T) Mn-AP XMCD. All curves have been normalized to the minimum of the experimental XMCD and are arbitrarily shifted in energy to align the theoretical to the experimental result. Features related to multiplet splitting effects are absent or smeared, as indicated by the vertical dashed lines. The interatomic screening and excessive electron-electron repulsion of the free ion were taken into account by reducing the Slater integrals to 80%. The 2p spin-orbit interaction was scaled to 103%. An exchange field of 0.01 eV was applied along the magnetization direction. The calculated spectra include a Lorentzian of 0.25 (0.4) eV for the $L_3(L_2)$ edge to account for intrinsic linewidth broadening and a Gaussian of σ=0.1 eV for instrumental broadening. For sake of comparison, all calculated spectra are normalized to the same amplitude and arbitrarily aligned in binding energy.

isolated ion in spherical symmetry,[24,26,27] and a d^5(50%)-d^6(50%) mixed-valence configuration. The d^5(50%)-d^6(50%) mixed-valence XMCD has been calculated within the impurity Anderson model with the additional parameters: $E_g(d^6)$=−3 eV, $E_f(d^6)$=−4 eV, and T_{t2g}=2T_{eg}=2. E_g and E_f are related to the charge-transfer energies for ground and excited states while T_{t2g} and T_{eg} are the charge-transfer integrals for t_{2g} and e_g orbitals, respectively.[28] Introducing in the calculation further d^4 character or d^4-d^5 mixing without d^6 terms does not provide any better agreement to the experimental Mn XMCD. The comparison to the calculation highlights the smearing of the multiplet features in the experimental results and reveals unambiguously that Mn-AP XMCD does not bear a pure atomiclike character, suggesting a mixed-valence state with itinerant character. Moreover, the broadened features at the high-energy side of the L_3 XMCD that appear for a metalliclike condition are totally absent, thus excluding Mn alloying/clustering. The observed mixed-valence features suggest a rearrangement of the local density of states associated to changes in the local Mn environment that may be interpreted by the formation of an impurity band, similar to half-metallic systems, where Mn atoms have localized magnetic moments but delocalized 3d electrons.[29,30]

To disentangle the Mn-AP ferromagnetic character from the paramagnetic one, we now need to assign the different contributions to the XMCD spectra. To this aim, a fitting procedure was performed, using a linear combination of ex-

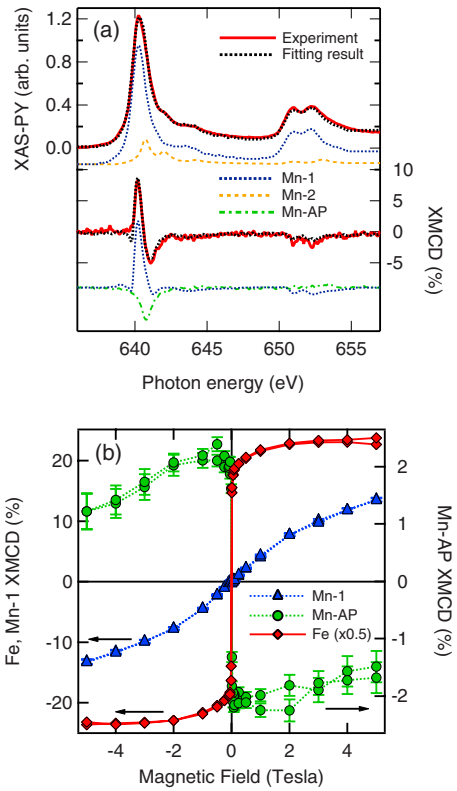

FIG. 3. (Color online) (a) Fitting results and experimental Mn $L_{2,3}$ XAS/XMCD spectra (black dashed curve and red/gray curve, respectively) using template spectra from Ref. 21 (Mn-1, blue/dark gray dashed curve and Mn-2 yellow/light gray dashed curve) and experimental Mn-AP XMCD (green/light gray dot-dashed curve). Experimental curves correspond to t(Fe)=23 ML, T=120 K, and H=1 T. Best agreement between experimental XMCD and fit is obtained by using only Mn-1 and Mn-AP component. (b) Hystereses cycles traced from the XMCD L_3 peak height at the Mn and Fe edges, in percentage of the XAS sum peak $(I_+ - I_-)/2$, for T=120 K, Fe=23 ML. Black arrows indicate the Fe XMCD scale (left) and Mn XMCD one (right). The Mn-1 (blue/dark gray triangles) and Mn-AP (green/light gray circles) hystereses were extracted by fitting the L_3 XMCD spectra at each magnetic field, using the same fitting procedure of panel (a) (linear combination of Mn-1 and Mn-AP components). The resulting Mn-1 behavior is purely paramagnetic, as expected above T_c of (Ga,Mn)As. Experimental values of Fe XMCD (red/gray diamonds) are multiplied by 0.5 for sake of comparison.

perimental Mn-1,2 XAS and XMCD spectra from Ref. 22, constrained to reproduce XAS and XMCD data vs magnetic field, temperature, and Fe thickness. The Mn-AP XMCD cannot be reproduced by the superposition of Mn-1 and Mn-2, and has to be explicitly included in the fitting routine. Results for 120 K, 1 T, and 23 ML of Fe are presented in Fig. 3(a). We find only two contributions in the XMCD spectra: paramagnetic from bulk Mn-1 ($T > T_c$) and ferromagnetic from Mn-AP. Although a 1 T field is applied, no paramagnetic contribution associated to Mn-2 character is found, thus confirming the absence of Mn oxide in the epitaxial HS. Disentangling the different Mn character in XMCD spectra allows tracing the evolution vs magnetic field, i.e., to reconstruct site selective (Mn-1 and Mn-AP) hysteresis loops, as

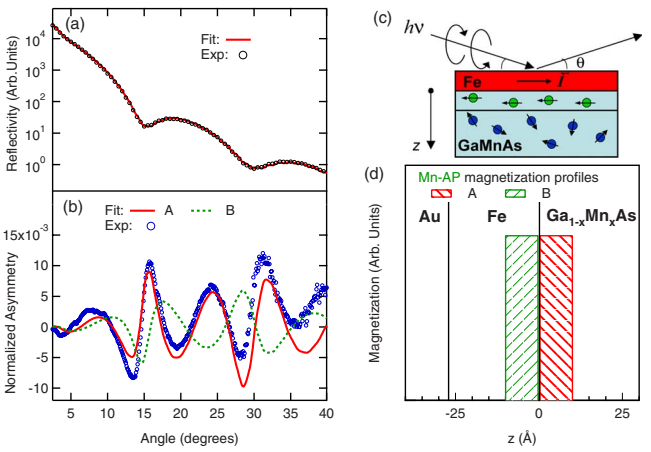

FIG. 4. (Color online) (a) Specular x-ray reflectivity at 138 K collected with a photon energy of 640.4 eV (black circles) compared with fitting results obtained with the PPM program (red/gray line). Values used in the fitting are (thickness and roughness in Å, respectively) (GaMn)As, 369 and 3.0. Fe 27 and 4.1. Au 41 and 2.1. GaAs substrate with roughness 1.0 Å. (b) Experimental asymmetry ratio AR (blue/dark gray circles), as defined in the text. Comparison of the experimental AR with two simulated magnetic profiles, i.e., a 10-Å-thick magnetic layer of Mn ions located in the (Ga,Mn)As environment (red/gray curve, panel d) or in the Fe film (green/light gray curve, panel d). (c) Sketch of the experimental geometry used for XRMS experiments.

presented in Fig. 3(b). The Mn-AP hysteresis matches the Fe one up to 2 T, indicating the robustness of the magnetic coupling. At higher magnetic fields the observed partial reduction in the Mn magnetic moment (≅40%) suggests a reorientation of the Mn magnetization in a direction parallel to the field. Having identified the novel magnetic and electronic behavior of Mn-AP, we now address the distribution profile of Mn-AP across the interface, by means of XRMS results. Figure 4(a) reports the θ-2θ scan obtained at $h\nu$=640.4 eV and T=138 K, averaging the reflectivity curves for parallel and antiparallel relative orientation of photon helicity and magnetic field. Such a signal is insensitive to the magnetic moments of the sample and depends only upon the electron charge distribution and chemical properties. In Fig. 4(b) we report the asymmetry ratio $AR = (r\uparrow\uparrow - r\uparrow\downarrow)/(r\uparrow\uparrow - r\uparrow\downarrow)$, where $(r\uparrow\uparrow)$ and $(r\uparrow\downarrow)$ are the reflectivity values measured for parallel and antiparallel orientation of the photon helicity and magnetization, respectively. The AR value gives information about the distribution of the Mn magnetic moment in the sample. We fitted the θ-2θ scan using the thickness and roughness of the various layers [Au,Fe,(GaMn)As,GaAs] as fitting parameters. Absorption coefficients for the Mn species have been obtained experimentally from XAS measurements. The real part of the refractive index is obtained from the imaginary part, which is directly proportional to the absorption coefficient, through Kramers-Kroenig transformation. The fitting results well reproduce the experimental curve (the values of the best fit parameters are listed in the caption of Fig. 4), in good agreement with TEM results. Considering a distribution of Mn atoms antiparallely oriented with respect to Fe, we are able to reproduce maxima and minima of the measured oscillations: best agreement is found

using a 10-Å-thick layer of Mn atoms with a constant steplike magnetic profile in (Ga,Mn)As. We also simulated the behavior of the same Mn thickness, but with Mn diffused into the Fe layer, in antiparallel configuration. The period of oscillations is almost equal but the positions of the maxima and minima are inverted. This excludes a sizeable presence of magnetic Mn atoms into the Fe film. We stress that the simple steplike magnetization profile used in the simulation, although able to reproduce the XRMS data, should be considered as a lower estimate of the Mn-AP magnetic depth profile.

IV. CONCLUSIONS

In conclusion, by the use of a broad range of chemical sensitive spectroscopic tools we have provided a complete description of the Mn magnetic properties in fully epitaxial Fe/GaMnAs HS. The use of the magnetic proximity effect between Fe and Mn made it possible to reveal a novel electronic configuration of the interfacial Mn atoms, with different magnetic behavior with respect to the bulk ones. Our original approach demonstrates that important insights in the fundamental interactions driving ferromagnetism in DMS-based systems can only be obtained by tailoring novel properties in controlled heterostructures. Future efforts in the direction of hybrid metal/DMS ferromagnetic structures may achieve the control of switching fields and Curie temperature, opening a completely new avenue for the design of hybrid metal/DMS/semiconductor structures for future spintronic devices.

ACKNOWLEDGMENTS

Financial support by the DFG through the SFB 689 is gratefully acknowledged. This work has been partially funded by CNR-INFM. Thanks are due to Alessandro Mirone for fruitful discussion and support for the use of the PPM code, and to Stefano Nannarone and Bruce A. Davidson for fruitful discussions on XRMS technique. A.V. was supported by the FVG Regional Project SPINOX funded by Legge Regionale 26/2005 and the decreto 2007/LAVFOR/1461.

*panaccioneg@elettra.trieste.it

[1] S. A. Wolf, D. D. Awschalom, R. A. Buhrman, J. M. Daughton, S. von Molnár, M. L. Roukes, A. Y. Chtchelkanova, and D. M. Treger, Science **294**, 1488 (2001).
[2] D. D. Awschalom and M. E. Flatté, Nat. Phys. **3**, 153 (2007).
[3] A. H. Macdonald, P. Schiffer, and N. Samarth, Nature Mater. **4**, 195 (2005).
[4] I. Zutic, J. Fabian, and S. Das Sarma, Rev. Mod. Phys. **76**, 323 (2004).
[5] G. Wastlbauer and J. A. C. Bland, Adv. Phys. **54**, 137 (2005), and references therein.
[6] K. Olejnik, M. H. S. Owen, V. Novák, J. Mašek, A. C. Irvine, J. Wunderlich, and T. Jungwirth, Phys. Rev. B **78**, 054403 (2008); J. Cryst. Growth **311**, 2151 (2009).
[7] J. Chakhalian, W. Freeland, H.-U. Habermeier, G. Cristiani, G. Khaliullin, M. van Veenendaal, and B. Keimer, Science **318**, 1114 (2007).
[8] H. Yamada, Y. Ogawa, Y. Ishii, H. Sato, M. Kawasaki, H. Akoh, and Y. Tokura, Science **305**, 646 (2004).
[9] C. Chappert, A. Fert, and F. Nguyen Van Dau, Nature Mater. **6**, 813 (2007).
[10] M. Zhu, M. J. Wilson, B. L. Sheu, P. Mitra, P. Schiffer, and N. Samarth, Appl. Phys. Lett. **91**, 192503 (2007).
[11] M. Zhu, M. J. Wilson, P. Mitra, P. Schiffer, and N. Samarth, Phys. Rev. B **78**, 195307 (2008).
[12] S. Mark, C. Gould, K. Pappert, J. Wenisch, K. Brunner, G. Schmidt, and L. W. Molenkamp, Phys. Rev. Lett. **103**, 017204 (2009).
[13] F. Maccherozzi, M. Sperl, G. Panaccione, J. Minár, S. Polesya, H. Ebert, U. Wurstbauer, M. Hochstrasser, G. Rossi, G. Woltersdorf, W. Wegscheider, and C. H. Back, Phys. Rev. Lett. **101**, 267201 (2008).
[14] F. Maccherozzi, G. Panaccione, G. Rossi, M. Hochstrasser, M. Sperl, M. Reinwald, G. Woltersdorf, W. Wegscheider, and C. H. Back, Surf. Sci. **601**, 4283 (2007).
[15] F. Maccherozzi, G. Panaccione, G. Rossi, M. Hochstrasser, M. Sperl, M. Reinwald, G. Woltersdorf, W. Wegscheider, and C. H. Back, Phys. Rev. B **74**, 104421 (2006).
[16] Fe growth on etched substrates results in a polycrystalline morphology, with high degree of magnetic disorder. In this case, no detectable XMCD at the Mn edge has been found.
[17] L. G. Parratt, Phys. Rev. **95**, 359 (1954) PPM code is available at http://www.esrf.eu/computing/scientific/PPM/ppm.html
[18] B. L. Henke, E. M. Gullikson, and J. C. Davis, At. Data Nucl. Data Tables **54**, 181 (1993).
[19] K. W. Edmonds, P. Bogusławski, K. Y. Wang, R. P. Campion, S. N. Novikov, N. R. S. Farley, B. L. Gallagher, C. T. Foxon, M. Sawicki, T. Dietl, M. Buongiorno Nardelli, and J. Bernholc, Phys. Rev. Lett. **92**, 037201 (2004).
[20] K. W. Edmonds, W. Edmonds, N. R. S. Farley, R. P. Campion, C. T. Foxon, B. L. Gallagher, T. K. Johal, G. van der Laan, M. MacKenzie, J. N. Chapman, and E. Arenholz, Appl. Phys. Lett. **84**, 4065 (2004).
[21] A. A. Freeman, K. W. Edmonds, N. R. S. Farley, S. V. Novikov, R. P. Campion, C. T. Foxon, B. L. Gallagher, E. Sarigiannidou, and G. van der Laan, Phys. Rev. B **76**, 081201(R) (2007).
[22] K. W. Edmonds, G. van der Laan, A. Freeman, N. R. S. Farley, T. K. Johal, R. P. Campion, C. T. Foxon, B. L. Gallagher, and E. Arenholz, Phys. Rev. Lett. **96**, 117207 (2006).
[23] F. Kronast, R. Ovsyannikov, A. Vollmer, H. A. Dürr, W. Eberhardt, P. Imperia, D. Schmitz, G. M. Schott, C. Ruester, C. Gould, G. Schmidt, K. Brunner, M. Sawicki, and L. W. Molenkamp, Phys. Rev. B **74**, 235213 (2006).
[24] G. van der Laan and B. T. Thole, Phys. Rev. B **43**, 13401 (1991).
[25] H. Ohldag, V. Solinus, F. U. Hillebrecht, J. B. Goedkoop, M. Finazzi, F. Matsukura, and H. Ohno, Appl. Phys. Lett. **76**, 2928 (2000).
[26] T. Cowan, *The Theory of Atomic Structure and Spectra* (Univer-

sity of California Press, Berkeley, CA, 1981).

[27] Systematic investigation of crystal-field effects that could lead to such XMCD curve did not produce better agreement with the experimental XMCD. Therefore the theoretical XMCD for a pure Mn d^5 ground state in Fig. 2 was obtained in O(3) spherical symmetry.

[28] F. M. F. de Groot, Coord. Chem. Rev. **249**, 31 (2005).

[29] J. Kübler, A. R. Williams, and C. B. Sommers, Phys. Rev. B **28**, 1745 (1983).

[30] N. D. Telling, P. S. Keatley, G. van der Laan, R. J. Hicken, E. Arenholz, Y. Sakuraba, M. Oogane, Y. Ando, K. Takanashi, A. Sakuma, and T. Miyazaki, Phys. Rev. B **78**, 184438 (2008).